JURNAL KARTIKA KIMIA

J. Kartika Kimia, Mei 2026, 9, (1), 150-161
Journal homepage: http://jkk.unjani.ac.id/index.php/jkk
P-ISSN: 2655-1322 E-ISSN: 2655-0938

Synthesis and Characterization of $Ca_2Al_2SiO_7:Pr^{3+}$ Photoluminescence Materials via Sol-Gel Method

Maura Vanessa[1], Nirwan Susianto[1], Aep Patah[2,*]
[1]Chemistry Study Program, Faculty Mathematics and Natural Sciences, Institut Teknologi Bandung, Jl. Ganesha 10, 40132 Bandung
[2]Research Division of Inorganic and Physical Chemistry, Faculty Mathematics and Natural Sciences, Institut Teknologi Bandung, Jl. Ganesha 10, 40132 Bandung
*E-mail: aep@itb.ac.id

DOI: https://doi.org/10.26874/jkk.v9i1.1093

Received: 29 December 2025, *Revised*: 16 June 2026, *Accepted*: 16 June 2026, O*nline*: 18 June 2026

Abstract

$Ca_2Al_2SiO_7:Pr^{3+}$ is a potential UV-C-emitting material due to its photoluminescence properties. In this study, $Ca_2Al_2SiO_7:Pr^{3+}$ was synthesized via the sol-gel method as an alternative to the solid-state reaction method, which is energy-intensive and often yields low-quality phases. The synthesized products appeared as white powders for the undoped samples and pale green powders for the Pr^{3+}-doped samples. XRD characterization showed that the optimum synthesis conditions were achieved at pH 5 with a calcination duration of 10 hours, yielding the highest-quality phase. Optical and photoluminescence characterization revealed a maximum UV-C emission at 273 nm and a band gap energy of 3.92 eV at a Pr^{3+} doping concentration of 7.25% moles.

Keywords: $Ca_2Al_2SiO_7$, photoluminescence, praseodymium, sol-gel, UV-C emission

1 Introduction

Over the past few decades, numerous researchers have investigated and synthesized a diverse range of inorganic photoluminescence materials. Among these are metal oxides and yttrium tantalate (Y_3TaO_7) doped by Eu^{3+}, synthesized by Borges et al. using the sol-gel method. This material emits light at a wavelength of 605 nm when excited at 360 – 529 nm and below 350 nm, which results from a mixture of charge transfer between the filled 2p shell of O^{2-} and the partially filled 4f shell of Eu^{3+}, as well as between Ta^{5+} and O^{2-}[1]. Another example is the core-shell structure $NaGdF_4:Yb,Tm@NaGdF_4$, obtained by Wu et al. through thermal decomposition, which emits light at 480 nm [2]. Phosphates such as $(Y_{0.95}Eu_{0.0})PO_4$ synthesized hydrothermally by Zou et al., emit light in the range of 591 – 618 nm with excitation at 224 – 230 nm, while β-$Ca_3(PO_4)_2$, developed by Meenambal and Kannan via coprecipitation, emits light from 480 to 656 nm when excited at around 980 nm [3,4]. Additionally, silicates like $Ca_{20}Al_{26}Mg_3Si_3O_{68}$ doped with Ce^{3+} and Tb^{3+}, synthesized by An et al. using high-temperature solid-state methods, emit light at 426 nm when excited at 374 nm [5]. Silicates are regarded as one of the most extensively studied inorganic materials. Their versatility has led researchers to combine silicates with calcium and aluminum oxides in various ratios, resulting in a subtype of material known as calcium aluminosilicate.

For applications in photoluminescence, researchers frequently utilize two types of calcium aluminosilicate: gehlenite ($Ca_2Al_2SiO_7$) [6–12] and anorthite ($CaAl_2Si_2O_8$) [13–15], both of which are doped with trivalent lanthanide ions. Gehlenite is often favored over anorthite as the host material, with praseodymium(III) ion (Pr^{3+}) being one of the most commonly used dopants. Researchers have successfully synthesized Pr^{3+}-doped gehlenite using a conventional solid-state method, which involves grinding the precursors—calcium oxide (CaO), aluminium oxide (Al_2O_3), and silica (SiO_2)—followed by calcination at high temperatures [16–18]. The final product has the ability to emit photoluminescence light at a wavelength of ~268 nm, approximately, which is in the UV-C range. The resulting material is capable of emitting photoluminescence light at an

approximate wavelength of 268 nm, which falls within the UV-C range. Previous studies indicate that UV-C light can inhibit bacterial growth [19,20], suggesting that Pr^{3+}-doped gehlenite may hold significant potential for antibacterial applications.

The solid-phase method previously used is considered inefficient due to its lengthy calcination times (ranging from 1 to 3 days) and high energy requirements (approximately 1400 °C) to achieve products with high homogeneity and crystallinity [18]. In response, an alternative approach known as the sol-gel method was developed. Recently, this sol-gel technique has been utilized to synthesize gehlenite doped with Eu3+. This method yielded highly pure and crystalline products after only 4 hours of calcination at a lower temperature of 1100 °C, making it significantly more efficient than the solid-state method [21]. Consequently, this research has implemented the sol-gel method to produce Pr^{3+}-doped gehlenite, aiming to enhance both crystallinity and homogeneity.

2 Materials and Methods

2.1 Materials

The precursors utilized in this study include 1.48 g (6.4 mmol) of calcium nitrate tetrahydrate ($Ca(NO_3)_2{\cdot}4H_2O$) and 2.34 g (6.4 mmol) of aluminium nitrate nonahydrate ($Al(NO_3)_3{\cdot}9H_2O$), both sourced from Supelco. Tetraethyl orthosilicate (TEOS) was acquired from Sigma-Aldrich, along with a concentrated ammonia solution (25% NH_3). Additionally, 0.06 g of boric acid (H_3BO_3), obtained from Merck, served as the flux. The Pr^{3+} dopant was prepared by dissolving 0.531 g of praseodymium oxide (Pr_6O_{11}, also from Sigma-Aldrich) in a 0.5 M aqueous solution of nitric acid (HNO_3).

2.2 Experimental procedure

The compound $Ca_2Al_2SiO_7:Pr^{3+}$ was synthesized using a sol-gel process derived from a method previously established by Cai et al. in 2011 [21]. The synthesis procedure is visually represented in the diagram found in Figure 1. Each synthesis condition was repeated a minimum of three times to ensure reproducibility and to evaluate the impact of varying conditions, as detailed in Table 2.1.

The synthesis process commenced by combining calcium nitrate and aqueous praseodymium nitrate in ethanol, with concentrations varied at 3.76%, 7.25%, and 10.49% moles (Equations S1 – S4). Subsequently, a solution of aluminum nitrate and boric acid, also dissolved in ethanol, was introduced, and the mixture was stirred for 15 minutes. According to a previous study by Cai, boric acid serves to facilitate the gelation process under lower pH conditions. Tetraethyl orthosilicate (TEOS) was then added, followed by the careful addition of 25% NH_3 to adjust the pH until a sol was formed. The sol was vigorously stirred at 80 °C until a transparent wet gel emerged. The wet gel was then dried at 120 °C for 48 hours, ground into a fine powder, and pre-annealed at 450 °C for 4 hours to eliminate excess solvent and nitrate ions. Finally, the material was calcined at 900 °C to yield the final product.

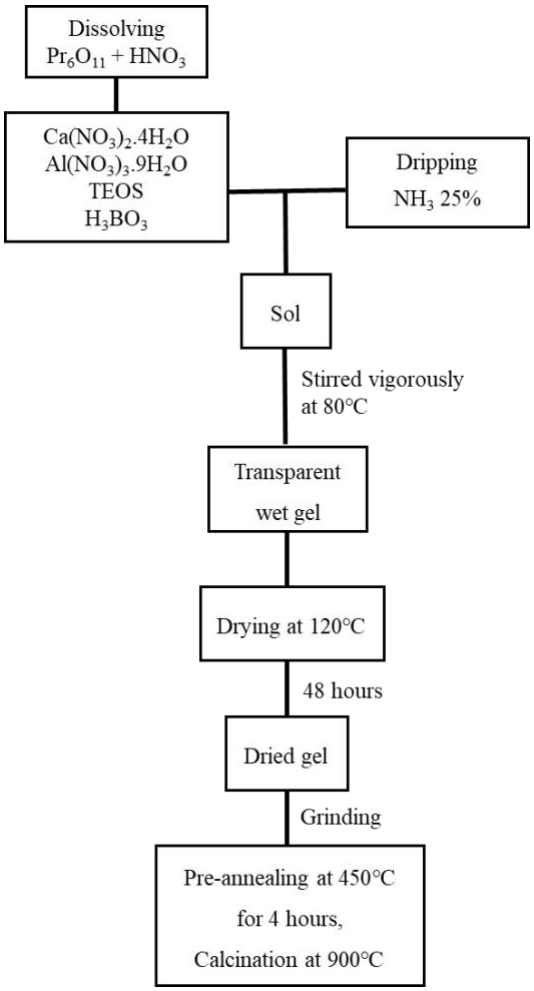


Figure 1. Schematic diagram for sol-gel synthesis of $Ca_2Al_2SiO_7:Pr^{3+}$

Table 1. Synthesis condition variation sets

Variation sets	Independent variables	Controlled variables	CODE
TEOS (mmol)	4.50	pH=5; 900°C-10h	CASO_TEOS(4.5)
	3.20		CASO_TEOS(3.2)
	1.80		CASO_TEOS(1.8)
pH	9	3.20 mmol TEOS; 900°C-10h	CASO_pH=9
	7		CASO_pH=7
	5		CASO_pH=5
Calcination time (hours)	24	pH=5; 3.20 mmol TEOS; 900°C	CASO_24h
	10		CASO_10h
	5		CASO_5h
%molesPr^{3+}	10.49	pH=5; 3.20 mmol TEOS; 900°C-10h	CASPr_10.49
	7.25		CASPr_7.25
	3.76		CASPr_3.76

2.3 Characterizations

The final product was characterized using a range of analytical techniques. X-ray diffraction (XRD, Rigaku MiniFlex 600) was employed to determine its crystalline structure. The surface morphology was examined via scanning electron microscopy (SEM, JEOL JSM-6510LA). Optical and photoluminescence properties were investigated using a UV–Vis Diffuse Reflectance Spectrophotometer (UV-DRS, Thermo Scientific Evolution 220) and a spectrofluorometer (FluoroMax), respectively. Additionally, Fourier-transform infrared spectroscopy (FTIR, Nicolet iS5 Thermo Scientific) was utilized to assess the vibrational characteristics of the product.

3 Results and Discussion

3.1 Structure and vibrational characteristics of $Ca_2Al_2SiO_7:Pr^{3+}$

Figure 2 exhibits a series of diffractogram patterns for each obtained $Ca_2Al_2SiO_7$ across 3 variation sets: the amount of TEOS used (1.80 – 4.50 mmol), pH condition (5 – 9), and calcination time (5 – 24 hours).

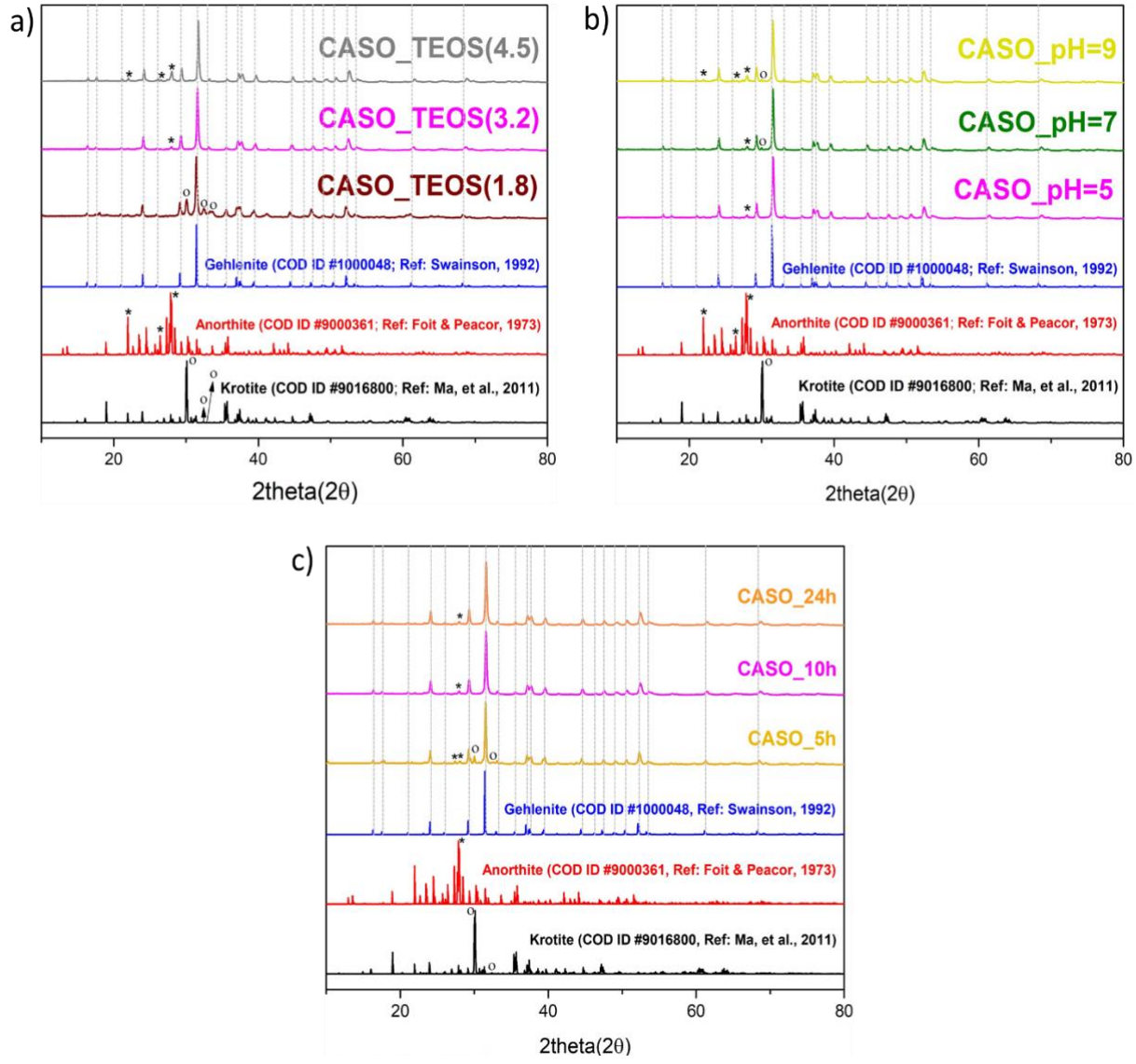


Figure 2. Diffractogram patterns for 3 variation condition sets of $Ca_2Al_2SiO_7$ (* = anorthite, O = krotite): a) TEOS variation set, b) pH variation set, c) calcination time variation set

As illustrated in Figure 2a, the XRD pattern of the product synthesized using 3.20 mmol of TEOS exhibits sharper peaks and aligns more closely with the reference, indicating a higher phase

quality compared to products synthesized with 1.80 mmol and 4.50 mmol of TEOS. When an excess amount of TEOS is utilized, it reacts with calcium and aluminum to form the anorthite ($CaAl_2Si_2O_8$) phase, which manifests as an impurity. This is particularly evident with the use of 4.50 mmol of TEOS, where three prominent anorthite peaks appear at 22.02°, 26.56°, and 28.06°. Additionally, there is a minor anorthite peak at 27.99° when 3.20 mmol of TEOS is employed. Conversely, when insufficient TEOS is present, the excess calcium and aluminum can lead to the formation of a krotite phase ($CaAl_2O_4$). This phase is observable when 1.80 mmol of TEOS is used, marked by peaks at 30.04°, 32.48°, and 33.72°.

Figure 2b illustrates that pH significantly influences the quality of $Ca_2Al_2SiO_7$, with values exceeding 5 leading to the formation of increased impurities. At a pH of 7, two small peaks emerged, identified as the anorthite and krotite phases. This phenomenon is attributed to the competition between $Al(OH)_3$ and Si–OH hydrolyzed species, which likely opened two pathways for the formation of anorthite and krotite. The anorthite phase was formed due to the interaction of Ca^{2+} ions with the aluminosilicate-rich coordination site, while the coordination of Ca^{2+} with the AlO_4^{5-} site resulted in the krotite phase. The intensity of these peaks slightly increases when the pH reaches 9. Under these conditions, an excess of hydrolyzed aluminum species is produced. Additionally, the hydrolysis of TEOS accelerates, resulting in the formation of reactive Si–OH species that combine with aluminum to generate more anorthite phase. However, a small amount of excess aluminum still interacts with Ca^{2+} ions to produce the krotite phase.

A shorter duration for calcination results in lower energy available for the formation of gehlenite, leading to a partial reassembly of Ca^{2+} and Al^{3+} into the krotite phase. Conversely, extending the calcination duration to 24 hours does not produce gehlenite that is significantly different from that obtained after 10 hours. It can therefore be concluded that the optimal conditions for synthesizing highly crystalline and homogeneous gehlenite involve using 3.20 mmol of TEOS at a pH of 5, with a calcination period of 10 hours. The synthesis of gehlenite doped with Pr^{3+} is carried out under these same conditions, varying the Pr^{3+} concentrations at 3.76%, 7.25%, and 10.49% as indicated by the calculations shown, with the corresponding diffraction patterns for each $Ca_2Al_2SiO_7:Pr^{3+}$ product presented in Figure 3.

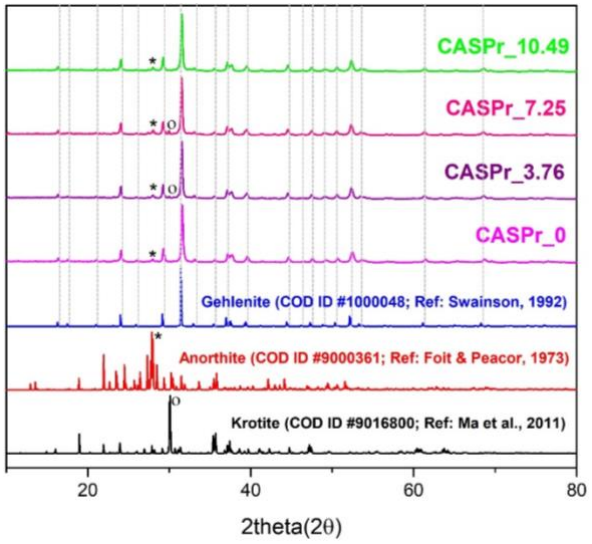


Figure 3. Diffraction patterns for $Ca_2Al_2SiO_7:Pr^{3+}$ (* = anorthite, O = krotite)

In examining the highest peaks of the presented diffractogram, it is observed that the incorporation of Pr^{3+} into gehlenite results in slightly shifted 2θ values. The principal peak for gehlenite, initially noted at 2θ = 31.59°, shifts towards lower angles upon Pr^{3+} doping, achieving values of 31.56°, 31.53°, and 31.55° for Pr^{3+} concentrations of 3.76%, 7.25%, and 10.49%, respectively This shift to lower 2θ values suggests lattice expansion due to the substitution of larger Pr^{3+} ions (1.126 Å) for Ca^{2+} ions (1.120 Å) [18], which aligns with Bragg's law.

Although the difference in ionic radii is minimal, the substitution of Pr^{3+} creates a charge imbalance that induces structural strain, leading to partial phase segregation of anorthite and krotite at intermediate doping levels, as the lattice strives for charge compensation. Notably, incorporating 10.49% Pr^{3+} moles indicates that the charge compensation mechanism becomes increasingly effective at higher dopant concentrations, which in turn stabilizes the anorthite phase.

The diffractogram was subjected to further analysis using the Rietveld method, with the resulting refinement outcomes presented in the Supplementary Information file (Figures S1-S4 and Tables S1-S4). Upon refining the obtained XRD patterns, both the undoped and doped gehlenite products were confirmed to possess the

same P-421m tetragonal crystal system, indicating that gehlenite remains the predominant crystalline component among all the phases. Additionally, the refined lattice parameters exhibit only minor variations, suggesting that the primary gehlenite crystal structure is resilient under the synthesis conditions investigated.

According to Table S1, the lattice parameters of $Ca_2Al_2SiO_7$ exhibited variation with the use of TEOS, indicating that the overall crystal structure remains intact across all conditions. However, the quality of refinement varied significantly; 3.20 mmoles of TEOS provided the best fit (R_p = 18.6%, Rw_p = 20.4%, χ^2 = 47.39), while both lower (1.80 mmol, χ^2 = 133.6) and higher (4.50 mmol, χ^2 = 132.1) amounts resulted in considerably poorer quality. This identifies 3.20 mmoles of TEOS as optimal for achieving a well-ordered fit for $Ca_2Al_2SiO_7$ formation. Table S2 illustrates that the lattice parameters of $Ca_2Al_2SiO_7$ remained nearly constant across a pH range of 5 to 9, confirming phase stability. Nonetheless, the quality of refinement progressively decreased from pH 5 to 9, suggesting that sol-gel synthesis in acidic conditions enhances the quality of the $Ca_2Al_2SiO_7$ phase. In relation to Table S3, an increase in calcination time led to a gradual contraction of the unit cell. A significant improvement in refinement quality was noted when extending the calcination from 5 hours to 10 hours, whereas further extension to 24 hours provided only marginal gains (χ^2 = 48.31), indicating that 10 hours is the optimal duration for achieving high quality in the $Ca_2Al_2SiO_7$ phase. Table S4 demonstrates that the lattice parameters of $Ca_2Al_2SiO_7$ remained stable across all Pr^{3+} concentrations, confirming successful substitution of Pr^{3+} at the Ca^{2+} sites. The refinement quality remained acceptable throughout (R_p: 18.6 – 24.3%; χ^2: 45.39 – 50.89), although a gradual decline was observed at higher doping levels, attributed to local strain and charge compensation effects stemming from the Pr^{3+}/Ca^{2+} charge imbalances.

The enhancement of the sol-gel method for synthesizing $Ca_2Al_2SiO_7$:Pr^{3+} with a high-quality phase was validated by comparing the diffraction patterns of the products obtained through the sol-gel method and the conventional solid-state method [22], as illustrated in Figures 4a and 4b. Both diffractograms reveal significant differences between the two methods; specifically, the sol-gel method yielded a product with higher crystallinity, approximately 92.23% for the undoped sample and 96.81% for the doped sample (data provided in Tables S5 and S6). In contrast, the product obtained via the conventional solid-state method exhibited a more amorphous structure, along with notable impurities. Due to the dominance of the amorphous phase, the crystallinity values from this method were deemed unreliable and are, therefore, not reported. Instead, a qualitative assessment of the XRD patterns was employed to evaluate the relative degree of crystallinity between the samples.

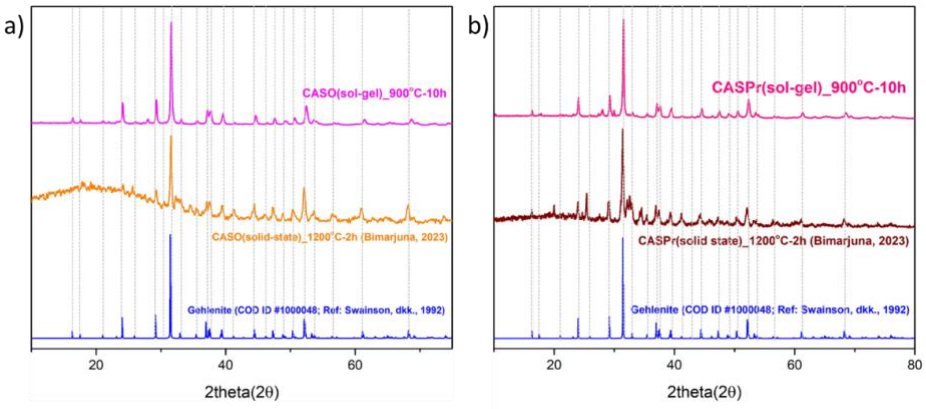


Figure 4. Diffractogram comparison of gehlenite sol-gel vs. solid state method: a)Undoped gehlenite, b)7.25%moles of Pr^{3+}doped gehlenite

The XRD analysis indicates that utilizing the solid-state method and calcining at 1200 °C for 2 hours led to the formation of gehlenite with significant impurity phases. This suggests an incomplete reaction, despite the high calcination temperature. This phenomenon can be attributed to the inherent microscale inhomogeneity associated with the mechanical mixing of the solid oxide precursors, which restricts interdiffusion even at elevated temperatures. In contrast, the sol-gel method, followed by calcination at 900 °C for 10 hours, yielded gehlenite of high quality, demonstrating that molecular-level mixing of the salt precursors within a solution effectively eliminates diffusion barriers and facilitates the complete formation of gehlenite at a significantly lower temperature. This evidence supports the conclusion that the sol-gel method is superior for achieving a high-quality phase while being more cost-effective due to the reduced calcination temperature and the absence of additional furnace costs, in contrast to the high-temperature solid-state calcination, which incurs greater expenses. The bond vibrational properties of $Ca_2Al_2SiO_7$ were assessed using FTIR, as displayed in Figure 5.

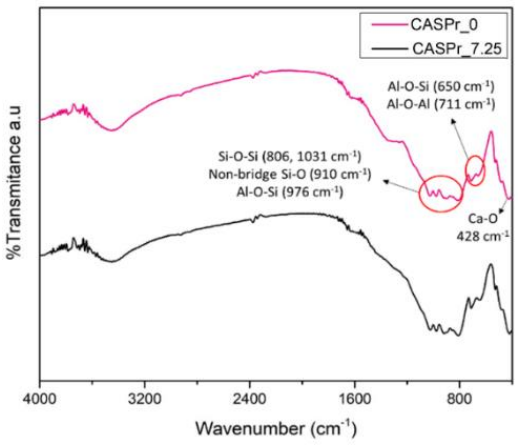


Figure 5. FTIR spectra for $Ca_2Al_2SiO_7$ host-material and doped with Pr^{3+}

The FTIR spectra exhibit Ca-O bond vibration at a wavenumber of 428 cm^{-1}, indicating a CaO_8 hendecadron structure. Besides, the existence of aluminosilicate polymeric structure is demonstrated through stretching mode of Al-O-Al bond from AlO_4 structure (711 cm^{-1}), bending (650 cm^{-1}) and stretching (976 cm^{-1}) modes of the Al–O–Si bond. The symmetric and asymmetric stretching modes of the Si–O–Si bond are observed at 806 and 1031 cm^{-1}, respectively, along with the stretching mode of non-bridge Si–O at 910 cm^{-1}. The addition of 7.25% moles of Pr^{3+} did not result in any significant changes to the spectra; however, upon closer examination of the wavenumbers, a slight shift is noted due to the charge imbalance between Ca^{2+} and Pr^{3+} ions. This imbalance affects the lattice distortions and bond lengths within the host structure.

3.2 Morphology of Ca2Al2SiO7:Pr3+

The obtained white powder of $Ca_2Al_2SiO_7$ host material and the green powder of $Ca_2Al_2SiO_7$ doped with 7.25% moles of Pr^{3+} were analyzed using Scanning Electron Microscopy (SEM) at a magnification of 20,000 to examine their morphologies. The SEM image of undoped gehlenite (Figure 6a) reveals an irregular, angular grain morphology characterized by a wide distribution of large, well-defined pores. The grains appear coarse and heterogeneous, indicating limited densification during the sintering process. The presence of large inter-granular pores suggests an open porous microstructure, which is typical of undoped gehlenite synthesized under these conditions.

In contrast, the gehlenite doped with Pr^{3+} (Figure 6b) exhibits a finer and more homogeneous microstructure. The grains are significantly smaller and more rounded compared to the undoped sample, with noticeably smaller pores as well. This morphological refinement implies that the incorporation of Pr^{3+} affects nucleation and growth, potentially inhibiting grain coarsening and promoting a more uniform microstructure during synthesis.

The SEM is subsequently analyzed using ImageJ to gather information on pore size distributions and porosity for each sample over a period of 10 hours. The observed differences between the two morphologies indicate that the

Pr^{3+} dopant plays a significant role in modifying the microstructural development of gehlenite. The reduction in grain size and changes in pore dimensions resulting from doping may enhance both optical and structural properties, as finer microstructures are typically linked to improved light scattering homogeneity and greater mechanical integrity.

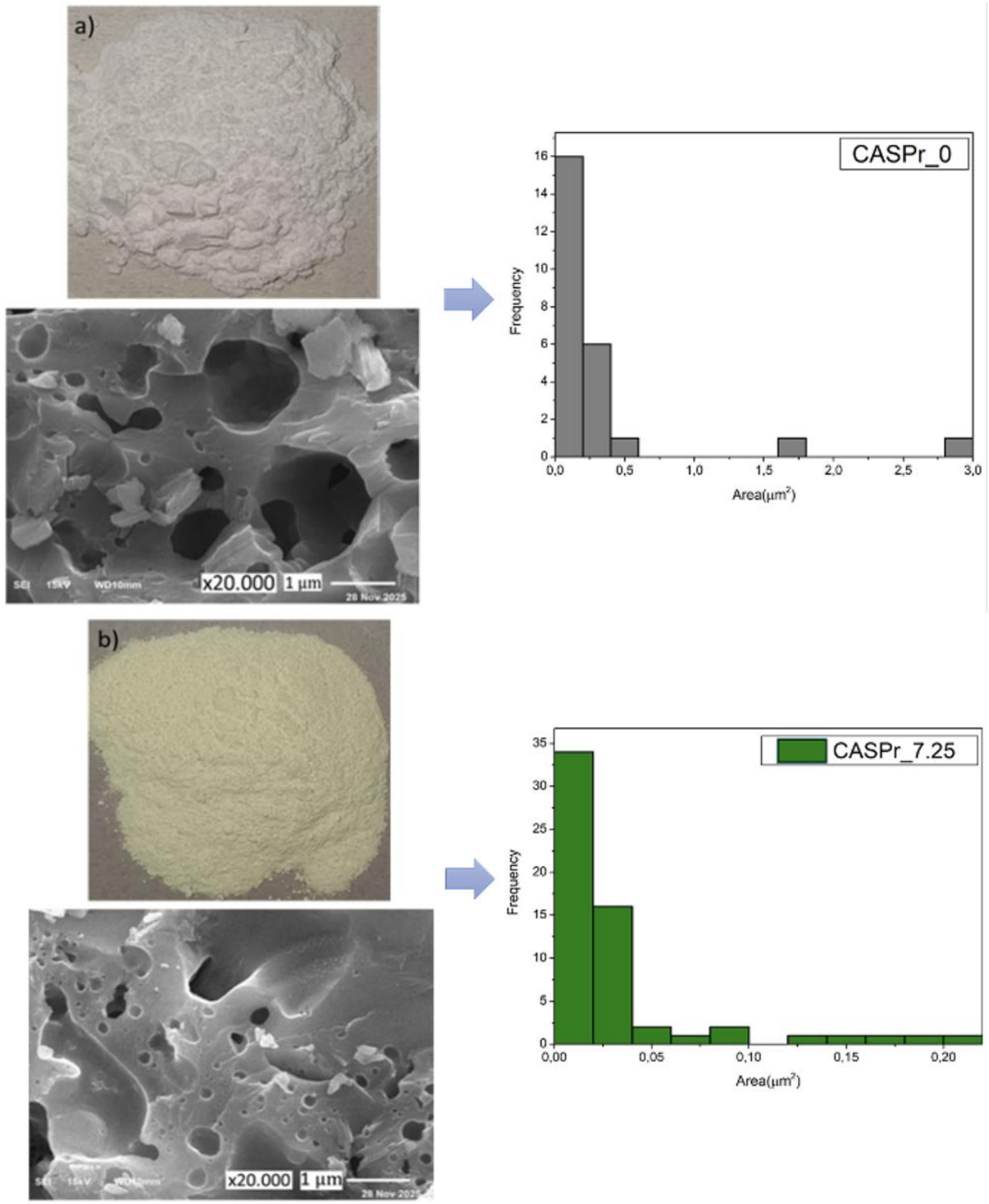


Figure 6. Morphology and pores size distribution of: a)$Ca_2Al_2SiO_7$, b)$Ca_2Al_2SiO_7$ with 7.25% moles Pr^{3+}

3.3 Optical and photoluminescence properties of Ca2Al2SiO7:Pr3+

The photoluminescence properties of the synthesized product, $Ca_2Al_2SiO_7:Pr^{3+}$, have been demonstrated through photoluminescence spectra, as illustrated in Figure 7a. Excitation from the $4f^2 \rightarrow 4f^15d^1$ state at a wavelength of 245 nm resulted in two emission peaks: one at 270 – 273.5 nm corresponding to the $4f^15d^1 \rightarrow 4H_{4,5,6}$ transition, and another at 317 – 320 nm for the $4f^15d^1 \rightarrow {}^3F_2$ transition, as referenced in Figure 7c, which aligns with the previously reported energy level diagram for Pr^{3+} [18]. The intensity of the emissions reached a maximum with the addition of 7.25% moles of Pr^{3+}. However, a quenching phenomenon was observed when the molar concentration of Pr^{3+} increased to 10.49%. This excessive introduction of dopant ions creates non-radiative energy transfer pathways, ultimately reducing luminescence efficiency. According to Blasse's formula, the critical distance (Rc) is approximately 12.48 Å, suggesting that the quenching effect is likely due to electric multipole-multipole interactions.

Figure 7b examines the synthesis method as a variable by comparing the optimal samples prepared through sol-gel and conventional solid-state sintering at 1200 °C for 2 hours [22]. The sol-gel method demonstrates significantly enhanced emission intensity at both 273.5 nm and 317 nm in comparison to the solid-state method. This improvement can be attributed to the molecular-level mixing inherent in the sol-gel process, which facilitates a uniform distribution of Pr^{3+} ions within the gehlenite host lattice, minimizes grain boundary defects, and lowers the crystallization temperature. In contrast, the high-temperature solid-state route results in a sample with markedly diminished luminescence, likely due to uneven dopant distribution and an increase in structural defects caused by the severe thermal conditions.

Further analysis of the optical properties of the obtained products was conducted using UV-DRS (Ultra-violet Diffuse Reflectance Spectroscopy). Figure 8 illustrates that the $Ca_2Al_2SiO_7$ host material exhibits maximal UV light absorption at a wavelength of approximately 203 nm, with its white color enhancing its ability to reflect the absorbed UV light, achieving a reflection rate of about 73.30%. Nevertheless, a shoulder peak emerges alongside the main peak, indicating a high surface area activity, which in turn leads to local structural disorder. This phenomenon is associated with the formation of localized energy levels at the maximum of the valence band (band edge).

The UV–DRS spectra and corresponding Kubelka–Munk plots for $Ca_2Al_2SiO_7:Pr^{3+}$ materials are illustrated in Figure 8. The optical band gap energy was estimated using the Kubelka–Munk theory, where the diffuse reflectance data were transformed into the Kubelka–Munk function, $F(R)$, based on the relationship:

$$F(R) = \frac{(1-R)^2}{2R}$$

where R represents the diffuse reflectance of the sample. The resulting $F(R)$ values were then correlated with photon energy (hν) through the Tauc plot relation for indirect electronic transitions:

$$(F(R).h\nu)^{1/2} = B(h\nu - Eg)$$

This approach indicates that gehlenite is classified as an indirect band gap material. The optical band gap (E_g) was determined by extrapolating the linear region of the Tauc plot toward the photon energy axis (as shown in Extrapolation 1 – 5). For the undoped sample, two absorption edges were identified, comprising a shoulder at 5.38 eV and a principal band gap at 5.65 eV. With the incorporation of Pr^{3+}, the band gap energy significantly decreased to 4.60 eV, suggesting the introduction of impurity levels that facilitate electronic transitions at lower energies. An additional reduction in band gap energy was noted for gehlenite doped with 7.25% moles of Pr^{3+}, reaching 3.96 eV, indicating an increased contribution from Pr-related states and lattice distortion effects. However, at a higher Pr^{3+} concentration of 10.49% moles, the band gap exhibited a slight increase to 4.27 eV. This phenomenon may be attributed to changes in crystal field interaction, variations in defect concentration, or the partial saturation of impurity states at elevated dopant levels. Overall, the doping of Pr^{3+} effectively modified the electronic structure of gehlenite, resulting in a narrowing of the optical band gap compared to the undoped sample.

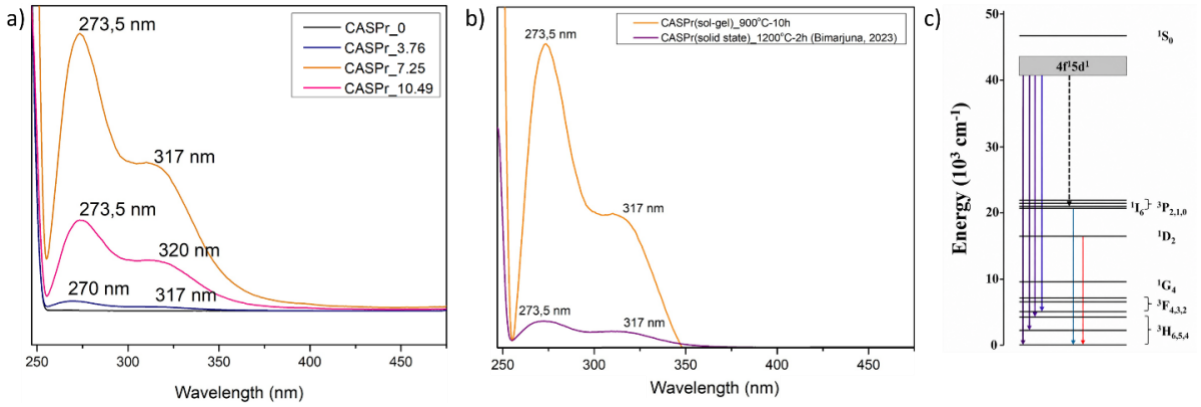


Figure 7. Comparison of photoluminescence emission intensities (excited at 245 nm); a)Addition of 3.76% – 10.49% moles of Pr^{3+}, b)sol-gel vs. conventional solid state method, c) Pr^{3+} energy transition (Nilova et al., 2021)

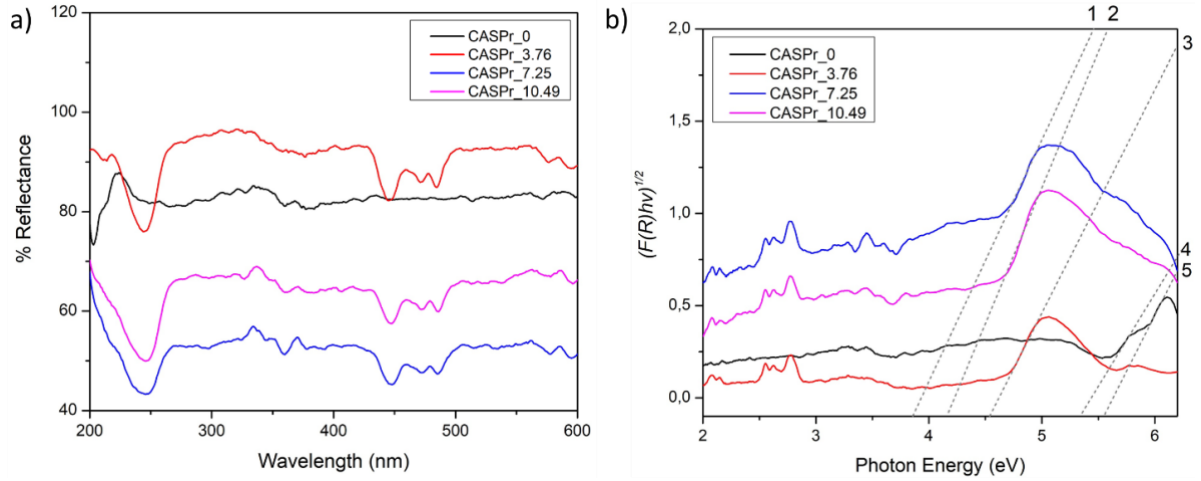


Figure 8. UV-DRS Analysis; a)Reflectance vs. wavelength plot of $Ca_2Al_2SiO_7:Pr^{3+}$; b)Kubelka-Munk plot and extrapolation of $Ca_2Al_2SiO_7:Pr^{3+}$

4 Conclusion

$Ca_2Al_2SiO_7:Pr^{3+}$ photoluminescence materials were successfully synthesized using a sol-gel method. The optimal synthesis condition was determined to be 3.20 mmol of TEOS at a pH of 5, followed by calcination at 900 °C for 10 hours. This process yielded a tetragonal gehlenite phase with relatively good crystallinity and minimal secondary phases. The incorporation of Pr^{3+} doping resulted in slight changes to the lattice parameters, indicating successful integration of Pr^{3+} into the $Ca_2Al_2SiO_7$ host lattice. FTIR spectra confirmed the presence of characteristic vibrations for Ca–O, Al–O, Si–O, and Al–O–Si bonds, while SEM images revealed porous, sponge-like particles. The strongest UV-C photoluminescence emission was observed in the sample doped with 7.25% moles of Pr^{3+}, exhibiting an emission maximum at approximately 273 nm, along with an estimated optical band gap of 3.96 eV. These findings suggest that sol-gel-derived $Ca_2Al_2SiO_7:Pr^{3+}$ is a promising candidate for a UV-C-emitting photoluminescence material. However, further investigations into emission stability, quantum efficiency, and antibacterial performance are essential to ascertain its practical applicability.

Acknowledgement

The authors would like to express their sincere and deepest gratitude to the AP Research Group for the invaluable guidance and support. This research was also made possible by generous funding from the Chemistry Study Program, Faculty of Mathematics and Natural Sciences,

Institut Teknologi Bandung (ITB). AP thanks ITB for partial financial support to this project through research funding with contract number 1687/IT1.B07.1/KU/2025.

References

[1]. Borges FH, Caixeta FJ, Pereira RR, de Oliveira SR, Gonçalves RR. Yttrium tantalate containing high concentrations of Eu^{3+} as dopant: Synthesis and structural and luminescence features. J Lumin. 2018;199:143–53.

[2]. Wu S, Meng Z, Sun X, Zhang S. Morphology control of the $NaGdF_4$:Yb,Tm@$NaGdF_4$ core-shell nanostructure by tailoring the ratio of core to shell. CrystEngComm. 2017; 19(34):1–7.

[3]. Meenambal R, Kannan S. Cosubstitution of Lanthanides (Gd^{3+}/Dy^{3+}/Yb^{3+}) in β-$Ca_3(PO_4)_2$ for Upconversion Luminescence, CT/MRI Multimodal Imaging. ACS Biomater Sci Eng. 2018;1–10.

[4]. Zou J, Zhu Q, Li X, Sun X, Li JG. Controlled hydrothermal processing of multiform $(Y_{0.95}Eu_{0.05})PO_4$ crystals and comparison of photoluminescence. J Alloys Compd. 2021; 870:1–11.

[5]. An Z, Zou H, Xu C, Zhang X, Dong R, Sheng Y, et al. $Ca_{20}Al_{26}Mg_3Si_3O_{68}$:$Ce^{3+}$,$Tb^{3+}$ Phosphors: Preferential Site Occupation, Color-Tunable Luminescence and Device Application. ACS Sustain Chem Eng. 2019;7:3154–63.

[6]. Tiwari G, Brahme N, Sharma R, Bisen DP, Sao SK, Sahu IP. $Ca_2Al_2SiO_7$:Ce^{3+} Phosphors for Mechanoluminescence Dosimetry. Luminescence. 2016;1–9.

[7]. Son NM, Tien DT, Lien NTQ, Quang VX, Trac NN, Hong TT, et al. Luminescence and Thermal-Quenching Properties of Red-Emitting $Ca_2Al_2SiO_7$:Sm^{3+} Phosphors. J Electron Mater. 2020;49(6):3701–7.

[8]. Trac NN, Van Tuyen H, Van Khoa Bao L, Vi NH, Thuan ANH. Energy level location of divalent and trivalent lanthanides in calcium aluminosilicate materials. J Mater Sci Mater Electron. 2021;32:4239–47.

[9]. Tien DT, Son NM, Nhat ND, Tuyen H Van, Ngoc LXD, Toan TQ. Energy-Transfer Phenomenon and Color-Tunable Properties of $Ca_2Al_2SiO_7$: Dy^{3+}/Eu^{3+} Phosphors. Hue Univ J Sci Nat Sci. 2023;132(1B):93–100.

[10]. Tuyen H Van, Vi NH, Bao LVK. Luminescence Quenching of Ce^{3+} and Energy Transfer Phenomenon in $Ca_2Al_2SiO_7$:Ce^{3+}, Sm^{3+} Phosphors. DTU J Sci Technol. 2020;04(41):46–52.

[11]. Abudouwufu T, Sambasivam S, Wan Y, Abudoureyimu A, Yusufu T, Tuxun H, et al. Energy Transfer Behavior and Color-Tunable Properties of $Ca_2Al_2SiO_7$:RE^{3+} (RE^{3+} = Tm^{3+}, Dy^{3+}, Tm^{3+}/Dy^{3+}) for White-Emitting Phosphors. J Electron Mater. 2018;1–8.

[12]. Zhao L, Mao J, Jiang B, Wei X, Yin M, Chen Y. A New Yellow Long Persistent Luminescence Phosphor $Ca_2Al_2SiO_7$:Eu^{2+},Tm^{3+} found by co-doping Ln^{3+} (Ln = Ce, Pr, Nd, Sm, Gd, Tb, Dy, Ho, Er, Tm, Yb, Lu) with Eu^{2+} in $Ca_2Al_2SiO_7$ host. J Lumin. 2018;6–10.

[13]. Drewry SM, Eccles LE, Sickafus KE, Wetteland CJ, Page K. Preparation of high-density anorthite ($CaAl_2Si_2O_8$) through solid-state synthesis and uniaxial hot-pressing. J Mater Sci. 2024;59:1184–95.

[14]. Wang Y, Wang Z, Zhang P, Hong Z, Fan X, Qian G. Preparation of Eu^{2+} and Dy^{3+} co-activated $CaAl_2Si_2O_8$-based phosphor and its optical properties. Mater Lett. 2004;58(26):3308–11.

[15]. Yu X, Xu X, Jiang T, Yu H, Yang P, Jiao Q, et al. Tunable color emitting of $CaAl_2Si_2O_8$: Eu, Tb phosphors for light emitting diodes based on energy transfer. Mater Chem Phys. 2013;139(1):314–8.

[16]. Wang X, Chen Y, Liu F, Pan Z. Solar-blind ultraviolet-C persistent luminescence phosphors. Nat Commun. 2020;11(1):1–8.

[17]. Zhao S, Kanwal S, Su W, Lin H, Han Z, Zhuang S, et al. Investigation of $Ca_2Al_2SiO_7$:Pr^{3+}/Gd^{3+} UV-B upconverting phosphor and its optical thermometric properties. Univ Shanghai Sci Technol. 2024;1–24.

[18]. Nilova D, Antuzevics A, Krieke G, Doke G, Pudza I, Kuzmin A. Ultraviolet-C Persistent Luminescence and Defect Properties in $Ca_2Al_2SiO_7$:Pr^{3+}. Inst Solid State Phys. 2021;1–20.

[19]. Blatchley ER, Brenner DJ, Claus H, Cowan TE, Linden KG, Liu Y, et al. Far UV-C radiation: An emerging tool for pandemic control. Crit Rev Environ Sci Technol.

2023;53(6):733–53.

[20]. Foschi C, Giorgi B, Ambretti S, Lazzarotto T, Violante FS. Real-Life Assessment of the Ability of an Ultraviolet C Lamp (SanificaAria 200, Beghelli) to Inactivate Airborne Microorganisms in a Healthcare Environment. Life. 2023;13:1–8.

[21]. Cai J, Pan H, Wang Y. Luminescence Properties of Red-Emitting $Ca_2Al_2SiO_7:Eu^{3+}$ Nanoparticles Prepared by Sol-Gel Method. Rare Met. 2011;30(4):374–80.

[22]. Bimarjuna B. Synthesis and Characterization of $Ca_2Al_2SiO_7:Pr^{3+}$ Photoluminescence Materials by Ball-Milling Method. Undergrad thesis. 2023;1–80.